frontiers in Earth Science

ORIGINAL RESEARCH
published: 28 July 2020
doi: 10.3389/feart.2020.00283

The Effect of Early Diagenesis in Methanic Sediments on Sedimentary Magnetic Properties: Case Study From the SE Mediterranean Continental Shelf

Nitai Amiel[1]*†, *Ron Shaar*[2] *and Orit Sivan*[1]

[1] The Department of Geological and Environmental Sciences, Ben-Gurion University of the Negev, Beersheba, Israel, [2] The Institute of Earth Sciences, The Hebrew University of Jerusalem, Jerusalem, Israel

OPEN ACCESS

Edited by:
Myriam Kars,
Kôchi University, Japan

Reviewed by:
Janna Just,
University of Bremen, Germany
Natascha Riedinger,
Oklahoma State University,
United States

***Correspondence:**
Nitai Amiel
Nitai.amiel@weizmann.ac.il

†Present address:
Nitai Amiel,
Department of Earth and Planetary Sciences, Weizmann Institute of Science, Rehovot, Israel

Specialty section:
This article was submitted to Sedimentology, Stratigraphy and Diagenesis, a section of the journal Frontiers in Earth Science

Received: 24 March 2020
Accepted: 18 June 2020
Published: 28 July 2020

Citation:
Amiel N, Shaar R and Sivan O (2020) The Effect of Early Diagenesis in Methanic Sediments on Sedimentary Magnetic Properties: Case Study From the SE Mediterranean Continental Shelf. Front. Earth Sci. 8:283. doi: 10.3389/feart.2020.00283

Microbial respiration in marine sediment can affect the magnetic properties of the sediment through a complicated interplay between reductive dissolution and authigenic precipitation of iron-bearing magnetic minerals. However, a direct link between the main diagenetic zones in the upper sedimentary column and sedimentary magnetic properties using high resolution multi parameter profiles has been demonstrated only in few studies. Here, we directly correlate early diagenetic processes and sedimentary magnetism using a composite high-resolution sedimentary record of pore water chemistry, solid phase chemical measurements and mineral-magnetic parameters. Measurements along the profiles include the entire redox cascade, from the water-sediment interface, down through the deep methanic zone, on a six-meter sediment core collected from the Southern Eastern Mediterranean continental shelf. The uppermost part of the sediment core, associated with oxic, nitrous, manganous, ferruginous, and sulfate reduction zones, is characterized by high ferrous iron and sulfate concentrations and high values of the measured magnetic parameters [susceptibility, Isothermal remanent magnetization (IRM) and Anhysteretic remanent magnetization (ARM)]. This layer is underlain by a sulfate-methane transition zone (SMTZ) that shows a significant decrease in magnetic parameters due to the dissolution of magnetic minerals. Below the SMTZ, the methanic zone has been assumed to be magnetically inactive under steady-state conditions. However, we observe in the upper methanic zone an increase in microbial iron reduction, coupled to an abrupt increase in magnetic parameters. Our data indicate that the observed increase in the magnetic signal is related to the precipitation of authigenic magnetic minerals. These diagenetic changes should be considered when interpreting paleomagnetic data, and highlight the potential to use high-resolution magnetic data as a proxy for identifying diagenetic processes.

Keywords: early diagenesis, sedimentary magnetism, porewater chemistry, methanogenesis, iron reduction

INTRODUCTION

Microbial respiration of organic debris in sediments is coupled to the reduction of electron acceptors along a cascade of decreasing free energy yield from oxygen reduction, followed by nitrate reduction, manganese and iron oxide reduction, then sulfate reduction, and finally, methanogenesis (Froelich et al., 1979). This respiration order predicts that the more favorable processes (with more negative Gibbs energy) would occur at shallower depths (Jorgensen, 2000). Therefore, these respiration processes define diagenetic zones associated with change in the chemical composition of the pore water (Berner, 1980; Canfield and Thamdrup, 2009).

The change in pore water chemistry due to the microbial respiration processes can cause also diagenetic changes in the mineralogy of the sediment. This can include dissolution and precipitation of iron-bearing magnetic minerals, which leave traceable magnetic fingerprints (signals) in the sediment (Lovley, 1991; Liu, 2004; Maloof et al., 2007; Rowan et al., 2009; Roberts, 2015). Thus, understanding and characterizing the link between geochemical pore water profiles, diagenetic zones, and sedimentary magnetic changes, is necessary for adequate interpretation of magnetic sedimentary data, and vice versa can enable new insights into the microbial activity in sediments.

Magnetic properties of the sediment and the assemblage of its magnetic particles can vary as a response to changes in sediment transport and deposition regime, but also due to diagenetic reactions, which evolve with burial (Liu et al., 2012). In the oxic zone, surface oxidation of detrital iron minerals, mainly maghemitization of magnetite, commonly occurs (Smirnov and Tarduno, 2000; Torii, 2011). In addition, iron-bearing minerals can precipitate in the oxic, nitrogenous, and manganous zones (which can overlap) as dissolved ferrous iron from underlying zones diffuses upward and reacts with dissolved oxygen, nitrate, or with oxide minerals, to form oxyhydroxides (Lovley et al., 1990; Cornell and Schwertmann, 2003). In the ferruginous zone, iron minerals undergo reductive dissolution by iron reducing bacteria oxidizing organic substrates, releasing ferrous iron into the pore water and triggering the precipitation of authigenic and/or biogenic minerals, mainly magnetite (Channell et al., 1982; Chang et al., 1987; Karlin et al., 1987; Lovley et al., 1987). Ferric iron appears in most aquatic systems as low-solubility iron oxide minerals. Thus, its reduction is a challenge to microorganisms, which need to breathe those minerals, rendering many of them effectively unavailable for reduction deep in sedimentary environments, and leading to the dominance of sulfate reducing bacteria at a certain depth (Shi et al., 2007). In the sulfate reduction zone, sulfide, the product of bacterial sulfate reduction, reacts also with the remnant of the ferric iron oxides, which have survived the dissolution in the upper sediment. This causes oxidation of the sulfide to sulfur intermediates (and then to sulfate and sulfide by disproportionation), reductive dissolution of the detritus iron oxides and liberation of dissolved ferrous iron into the porewater (Rickard and Luther, 2007). The excess sulfide and the dissolved ferrous iron precipitate as authigenic iron-sulfide minerals, first as iron-monosulfide, altering to pyrite, the most stable iron-sulfide mineral, as sulfide concentration increases (Berner, 1984; Canfield and Berner, 1987; Roberts, 1995; Rowan et al., 2009).

Once sulfate is depleted, methane production by methanogens (Archaea), traditionally serves as the terminal process anchoring carbon remineralization. When the produced methane comes into contact with an available electron acceptor, it can be consumed by it through microbial oxidation (methanotrophy), the main process by which methane is prevented from escaping to the atmosphere. In marine sediments (the main natural reservoir of methane), up to 90% of the upward methane flux is consumed anaerobically by sulfate (Valentine, 2002), wherein established (diffusive) profiles it occurs within a distinct sulfate-methane transition zone (SMTZ). According to the classical view, minor magnetic changes are expected below the SMTZ with regard to the iron mineral assemblages in the sediments. A significant iron reduction has been recently reported below the SMTZ, in the methanic zone of marine sediments, where the release of dissolved ferrous iron often coincides with a decrease in methane concentrations (Jørgensen et al., 2004; März et al., 2008; Slomp et al., 2013; Riedinger et al., 2014; Treude et al., 2014; Egger et al., 2015). These observations suggest the possibility of a "deep" diagenetic zone associated with the reduction of iron minerals that have survived the upper reduction zones and potentially the formation of magnetic authigenic minerals.

Several studies have explored the relationship between porewater chemistry, sediment chemistry, and sedimentary magnetism (Kasten et al., 1998; Liu, 2004; Riedinger et al., 2005; Kawamura et al., 2007, 2012; Larrasoaña et al., 2007; Fu et al., 2008; März et al., 2008; Rao et al., 2008; Cruz et al., 2018). However, a direct link between depth profiles of chemical composition of the porewater and the magnetic parameters throughout the diagenetic zones has been only partly established (Garming et al., 2005; Fu et al., 2008). Here, we explore the coupling between porewater chemistry and sedimentary magnetism in marine sediments and investigate the entire diagenetic profile from the oxic zone down to the deep methanic zone.

MATERIALS AND METHODS

Study Site

The sediment core was collected from Station SG-1 (32°57.83′N 34°55.29′E), located on the continental shelf of Israel, 20 km offshore Acre, at a water depth of 85 m (**Figure 1**). The sediments in this area mainly correspond to input from the Nile River, which has been delivering a massive load of siliciclastic clays through counter-clockwise currents parallel to the coast since sea level stabilization at 6000–7000 years BP (Nir, 1984; Lambeck and Purcell, 2005; Schattner et al., 2010). The sediment extending 3–5 km from the shore is mainly composed of sand and silt, while further, the sediment is composed of muddy clayey sediments derived from the Nile. The most abundant clay mineral is montmorillonite (with a smaller fraction of illite and kaolinite), which makes silica, alumina, and ferric iron oxides the main chemical components in the bulk sediment (Nir, 1984). Although methane is not expected in the upper several meters

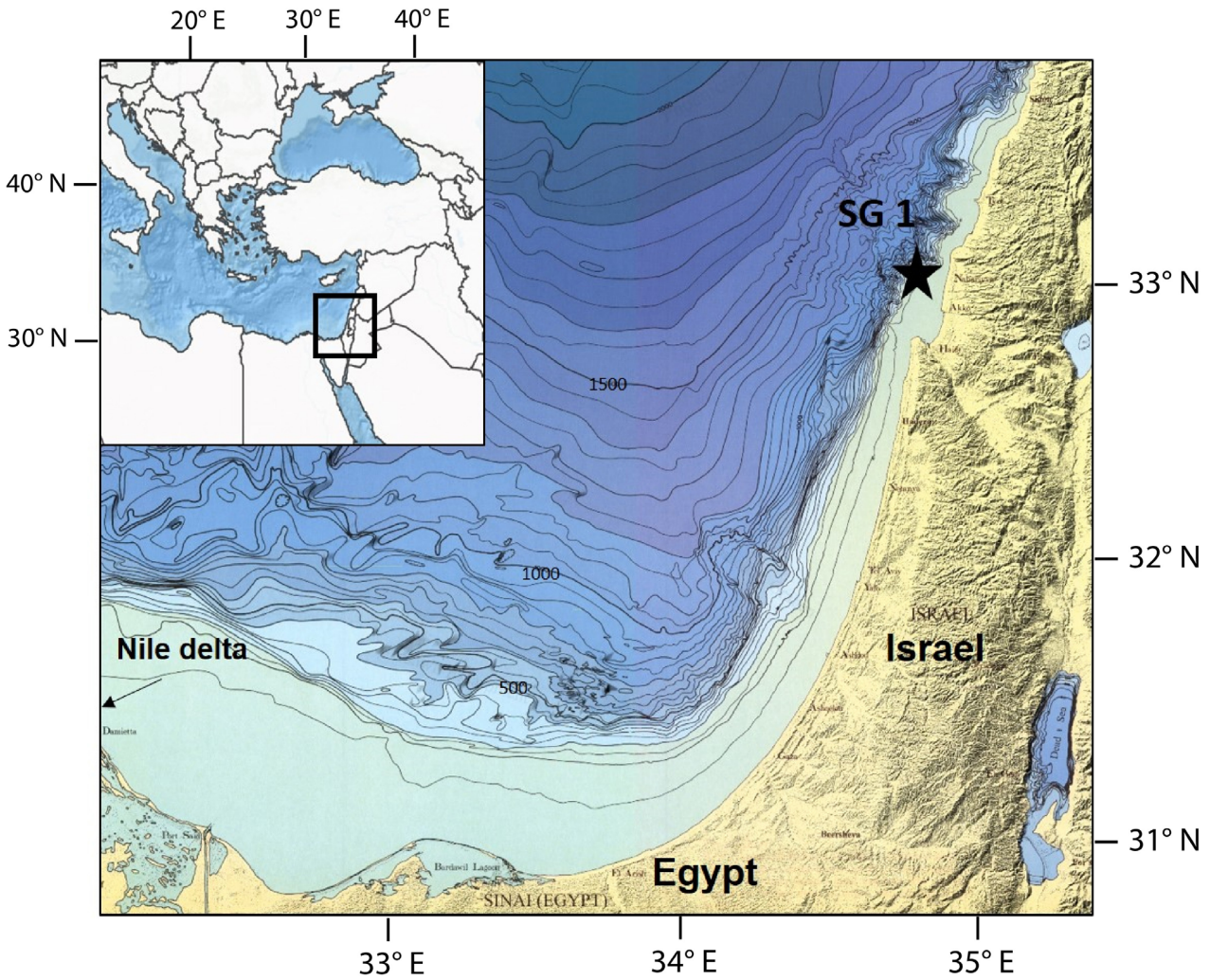

FIGURE 1 | Location map of Station SG-1 in the Southern Eastern Mediterranean Sea continental shelf.

of the sediments due to the oligotrophic characteristics the SE Mediterranean Sea surface water, methane was observed in several cores collected from SG-1 (Sela-Adler et al., 2015; Vigderovich et al., 2019; Wurgaft et al., 2019). They identified the SMTZ in the upper few meters of the sediments, conducted an isotopic analysis of the methane and concluded that most of the methane is from biogenic source and that it is being produced *in situ*. Yet, it is possible some methane gas might diffuse upward from a deeper biogenic methane gas pocket, which was observed by seismic surveys at depths of 40–110 m (Schattner et al., 2012).

Sampling

A 6 m long sediment core was collected from Station SG-1 using a piston corer during a cruise on the *R. V. Bat-Galim* in January 2017. The sediment core was sliced onboard at intervals of 30 cm within minutes of core collection. For headspace measurements of CH_4, approximately 1.5 mL of sediment was taken from the top of each sediment slice. This sediment was transferred immediately into N_2-flushed crimped bottles containing 5 mL of 1.5 N NaOH. Sediment samples from the top 5 cm of each sediment slice were transferred to vials under anaerobic conditions, and porewater was extracted from them on the same day by centrifugation at 4°C under an N_2 atmosphere. The supernatant was filtered through a 0.22 μm filter and was analyzed for dissolved Fe^{2+}, sulfide, and sulfate. The sediment was dried in an ambient temperate under N_2 atmosphere, the dry sediment was analyzed for different iron minerals fractions following the sequential extraction protocol from Poulton and Canfield (2005). The 30 cm core segments were split along their length and sampled for magnetic analysis by pushing non-magnetic plastic sampling boxes of 23 × 23 × 19 mm into the split halves at ∼5 cm intervals. Magnetic mineral extractions for scanning electron microscopy (SEM) were prepared from a mixture of 2–3 g of sediment and alcohol, using a strong hand magnet within a plastic probe (Nowaczyk, 2011). The extracts were dried in ambient temperature, half of the dried sediment was characterized by X-Ray Diffraction (XRD) measurement, the other half tapped on a conductive polycarbonate tape for

electron microscopy imaging and elemental analyses, using high-resolution SEM with an integrated energy dispersive X-ray spectroscopy (EDS).

Chemical Measurements

Headspace methane concentrations were measured on a Thermo Scientific gas chromatograph (GC) equipped with a flame ionization detector (FID) at a precision of 2 $\mu mol \cdot L^{-1}$. Sulfate concentrations were analyzed by inductively coupled plasma-atomic emission spectroscopy (ICP-OES-720-ES, VRIAN) with a precision of 2%. Ferrous iron was fixed immediately using Ferrozine solution, and its absorbance in 562 nm was measured on a spectrophotometer (Stookey, 1970), with an error of less than 7 $\mu mol \cdot L^{-1}$. Sulfide was measured using the Cline method (Cline, 1969), and 1.5 mL filtered porewater was inserted into a 15 mL falcon tube with 0.1 mL of ZnAc (200 $g \cdot L^{-1}$). Then, 120 μL of the diamine reagent was added into the solution, and the sample was stored in the dark for 30 min before measuring. Sulfide concentration was measured photometrically at 665 nm wavelength with a precision of $\pm$ 2%. The measurements of different iron minerals in the solid phase were performed on chemical extractions of four Fe fractions (Fe_{carb}- siderite and ankerite, Fe_{ox1}- ferrihydrite and lepidocrocite, Fe_{ox2}- goethite, hematite and akageneite, and Fe_{mag}- magnetite), following the Poulton and Canfield (2005) sequential extraction protocol. A 0.5 g dry sediment was inserted into a centrifuge tube with 10mL of a specific extractant at every stage. The fluids were separated from the sediment by centrifugation and removed from the tube after every extraction stage. At the end of each extraction stage, the extractant was transferred into a falcon tube containing ferrozine solution, and then it was measured spectrophotometrically. Fe_{Carb} was extracted by adding 1 M sodium acetate at pH 4.5 to the samples for 24 h. Fe_{ox1} was extracted by adding 1 M hydroxylamine- HCl in 25% [v/v] acetic acid to the samples for 48 h. Fe_{ox2} was extracted by adding 50 $g \cdot L^{-1}$ sodium dithionite buffered to pH 4.8 with 0.35 M acetic acid or 0.2 M sodium citrate for 2 h. Fe_{mag} was extracted by adding 0.2 M ammonium acetate solution at pH 3.2 for 6 h.

Magnetic Measurements

Magnetization measurements were carried out using a three-axial 2G-750 Superconducting Rock Magnetometer (SRM) system with an in-line two-axial AF unit and an axial anhysteretic remanent magnetization (ARM) coil. IRM was acquired using ASC pulse magnetizer and was measured using AGICO JR-6 spinner. Each sample was subjected to the following procedure: AF demagnetization of the NRM; ARM acquisition in 100 mT AC field and 0.1 mT bias field; AF demagnetization of the ARM using the same steps as the NRM demagnetization; IRM acquisition in 1.5 T. Demagnetization experiments were done in 11 steps (5, 10, 15, 20, 30, 40, 50, 65, 80, 100, 110, and 120 mT). Demagnetization data were analyzed using the PmagPy software package (Tauxe et al., 2016). Characteristic remanent magnetization (ChrM) directions were calculated from principal component analysis (PCA) following Kirschvink (1980). To detect the presence of gyro-remanent magnetization (GRM), typical to SD greigite (Snowball, 1997; Roberts et al., 2011) we calculate a GRM(%) parameter as described in eq. 1:

$$GRM(\%) = 100 \cdot \frac{m_{120\ mT} - m_{min}}{NRM} \quad (1)$$

Where $m_{120\ mT}$ is the magnetic moment after the 120mT step and m_{min} is the minimum moment measured during the AF demagnetization process.

Bulk low frequency (χlf) and high frequency (χhf) susceptibility were measured using an AGICO MFK-1 kappabridge at frequency of 976 and 15616 Hz, respectively. Frequency-dependent susceptibility (χfd) was calculated using the percentage of the normalized difference in susceptibility, as shown in eq. 2:

$$\chi_{fd}(\%) = 100 \cdot \frac{\chi_{lf} - \chi_{hf}}{\chi_{lf}} \quad (2)$$

High-temperature susceptibility thermomagnetic curves were measured on selected samples from depths 160, 280, 340, and 550 cm with the kappabridge using a CS4 furnace at temperatures ranging from ambient temperature to 700°C in Argon atmosphere. Low-temperature zero field cooling (ZFC) heating curves were measured on samples from depths 54, 150, 240, 350, 450, and 560 cm using Quantum Design MPMS by heating the samples under 10 mT magnetic field from 5K to room temperature after cooling them in zero field.

Electron Microscopy

Imaging of magnetic minerals, extracted from depths 84, 160, and 280 cm, was done using a FEI Magellan TM 400L field emission XHR-SEM (Oxford Instruments, United Kingdom) at 10–15 kV and 0.2 nA using a Secondary electron detector (ETD) and High contrast retractable solid-state detector (vCD). Elemental composition measurement was carried out using an energy dispersive X-ray spectroscopy (EDS) silicon drift detector Oxford X-Max (Oxford Instruments, United Kingdom). Imaging was conducted at the center of Nanoscience and Nanotechnology at the Hebrew University, Jerusalem, Israel.

X-Ray Diffraction

Sample characterization was performed by X-Ray Powder Diffraction method. Data were collected on Panalytical Empyrean Powder Diffractometer equipped with position sensitive detector (PSD) PIXCEL and Graphite monochromator on the diffracted beam The Cu K_α radiation (α = 1.541 Å) was used at operation conditions (voltage and current) 40 kV and 30 mA. The usual Bragg-Brentano q/2q was employed. q/2q scans were run for 15 min in a 2q range of 5–60° with step equal to ∼0.026°. Phase identification was performed by using the Match computer search/match program coupled with the ICDD (International Centre for Diffraction Data) Powder Diffraction File database (2015).

RESULTS

Sediment Composition

The sediment is composed of homogenous dark-gray clay and silt. Neither changes in grain size, nor in sediment color are visible. The XRD results (**Supplementary Figure S1**) indicate that the sediment is composed of quartz, calcite, clays, and albite. All four samples, collected from different depths, show an identical composition. Wurgaft et al. (2019) determined the content of calcite, clays, and quartz, in a different core collected from the same station, by 4–6%, 50–70%, and 15–25%, respectively. Measurements of iron fractions using chemical extractions (**Figure 2D**) show that goethite, hematite and akageneite (Fe_{ox2}) are the most abundant Fe minerals in the sediment, with concentrations of 2.2% wt/dry sediment at the top of the sediment, decreasing to 1.4% wt/dry sediment at 500 cm depth. Ferrihydrite and lepidocrocite (Fe_{ox1}) and siderite and ankerite (Fe_{carb}) concentrations at the sediment-water interface are 0.5 and 0.3% wt/dry sediment, respectively. Fe_{Ox1} concentration increases to 0.65% wt/dry sediment at 250 cm depth and then decreases to its initial value, while Fe_{carb} concentrations increase with depth to a value of 0.48% wt/dry sediment at 500 cm depth. Magnetite (Fe_{mag}) concentration decreases from 0.14% wt/dry sediment at the top of the sediment to 0.08% wt/dry sediment at 200 cm depth, then it rises to ∼0.18% wt/dry sediment between 220 and 260 cm, and decreases back to 0.1% wt/dry sediment below that.

Porewater Chemistry

Figures 2A–C shows the porewater chemistry depths profiles. Dissolved ferrous iron concentrations at the top 90 cm of the core are 20–90 μM, between 190 to 290 cm depth the concentrations are 20–70 μM, and at the rest of the core they are below 5 μM (with one exception at 480 cm depth) (**Figure 2A**). Sulfate concentrations are 34 mM at the top of the core, and gradually decrease to zero at 180 cm depth (**Figure 2B**). Methane starts to accumulate below 100 cm to ∼2.7 mM at 450 cm depth, where it remains stable with depth (**Figure 2C**).

According to the porewater chemistry data (**Figure 2**), the ferruginous zone is located at depths of 10–100 cm; the sulfidic zone is at the upper 180 cm; the SMTZ is located at depth of 105–180 cm, with a decrement in sulfate concentration parallel to the rise in methane concentrations; and the methanic zone is below 180cm with some peaks of iron reduction (see Discussion).

Rock Magnetism

Depth profiles of selected bulk rock magnetic parameters are shown in **Figures 2E–J**. For a detailed review of each of these parameters, see Liu et al. (2012). The Mass normalized low-frequency susceptibility χlf (**Figure 2E**, see section "Materials and Methods") is sensitive to the mineralogy and the concentration

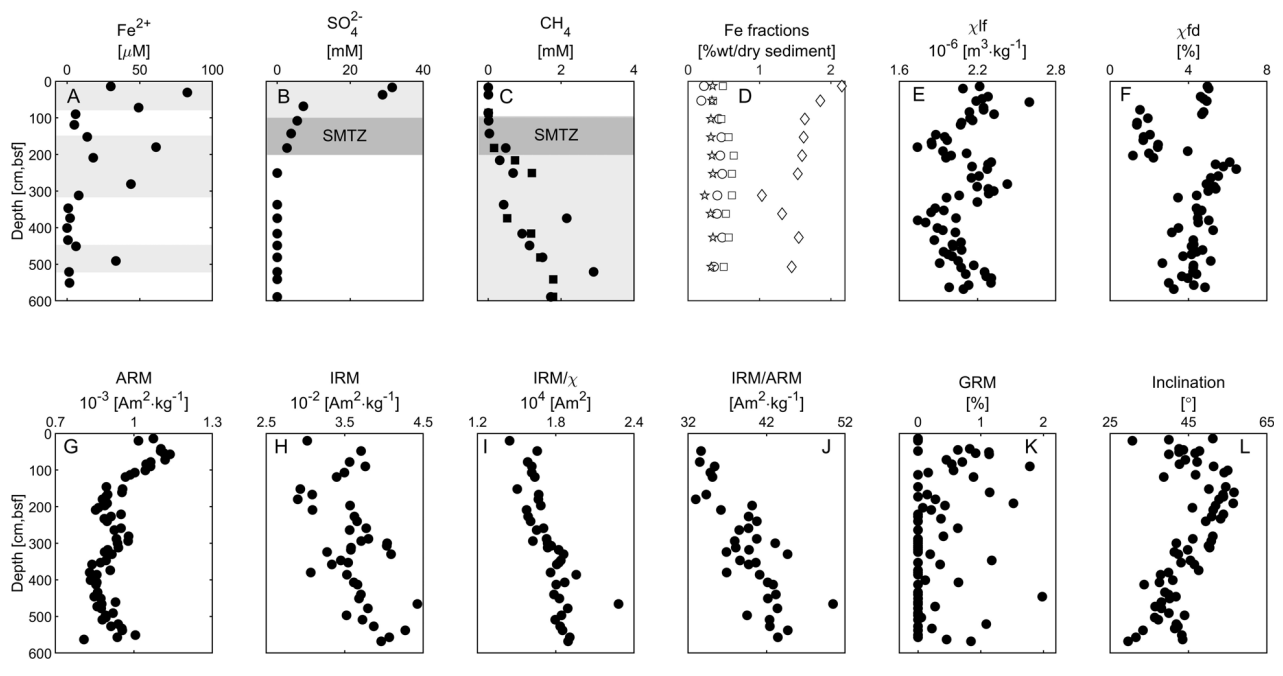

FIGURE 2 | Depth profiles of porewater geochemistry, Fe fractions, and magnetic data. **(A)** Porewater ferrous iron concentrations. **(B)** Porewater sulfate concentrations. **(C)** Porewater methane concentrations. **(D)** Sediment Fe fraction concentration. Fe_{carb} (siderite and ankerite) - Circles. Fe_{ox1} (ferrihydrite and lepidocrocite)- Squares, Fe_{ox2} (goethite, hematite, and akageneite)- Diamonds, Femag- Stars. **(E)** Low-frequency susceptibility. **(F)** Frequency dependent susceptibility. **(G)** Anhysteretic remanent magnetization (ARM), **(H)** Isothermal remanent magnetization (IRM). **(I)** IRM to low-frequency susceptibility ratio. **(J)** IRM to ARM ratio. **(K)** Gyroremanent magnetization (GRM%). **(L)** Inclination. The data in panels **(A–C)** represent the average of duplicates with error values smaller than the sample symbol, except the methane profile, in which the two duplicates are shown (in squares and circles). Iron and sulfate reduction and methanic zones are marked with gray background. The SMTZ is marked with dark gray background.

of all the magnetic phases. χlf shows a zigzagged pattern with two maxima at the top 100 cm and between ∼200–300 cm, and two minima at ∼150 cm and ∼380. The mass normalized ARM and IRM magnetizations (see Methods, **Figures 2G,H**) are sensitive to the mineralogy, grain size, and concentration of the ferromagnetic phase, and they show similar trends of changes as χlf. This indicates that the depth variations in the susceptibility and magnetization curves are affected mainly by changes in the properties of low coercivity ferromagnetic particles capable of recording both ARM at 100mT and IRM at 1.5T. χfd (**Figure 2F**) - the difference between the low-frequency and high-frequency susceptibilities (see Methods) - is sensitive to concentration of small sub-micrometer scale ferromagnetic particles across the superparamagnetic (SP) – single domain (SD) transition. The χfd shows a similar trend as χlf in the top 300 cm, but with more abrupt change at ∼100 cm and 210 cm. This indicates a sudden drop in the concentration of the smallest ferromagnetic particles below the upper 100 cm, and recovery of small particles below 210 cm. The ratio between IRM and ARM (**Figure 2J**) increases with depth, suggesting a steady increase in the grain size of the ferromagnetic particles below the SMTZ. The ratio between IRM and χlf (**Figure 2I**), which is sensitive to SD ferromagnetic mineralogy, and also used as an indicator to greigite (Roberts, 1995; Sagnotti and Winkler, 1999) also shows a steady increase with no abrupt changes. The AF median destructive field (MDF) of the ARM (not shown in **Figure 2**) ranges between 17.1mT and 19.0mT. We could not see any correlation between the MDF values and the rest of the magnetic parameters.

The thermomagnetic curves of all four measured samples show very similar patterns (**Figure 3**). The susceptibility values gradually decrease above 400°C, with sharp drops between 400°C and 500°C and near 580°C. This indicates the presence of magnetite and titanomagnetite.

The ZFC curves (**Figure 4**) can help identify the presence of stoichiometric magnetite using the Verwey transition, the change in magnetite magnetization due to a crystallographic phase transition from an inverse cubic spinel to monoclinic, which occurs at 124 k (Verwey, 1939). The curves (**Figures 4A–F**) show similar trends, dominated by a paramagnetic signal that apparently masks small changes in magnetization. An increase in magnetization between 25K to 50K is observed in all samples. In order to detect small changes in magnetization around the Verwey transition temperature, which are not clearly visible in **Figures 4A–F**, we show in **Figure 4G** the first derivative of the ZFC curves. A peak in the derivative near the Verwey transition temperature, which is indicative for the presence

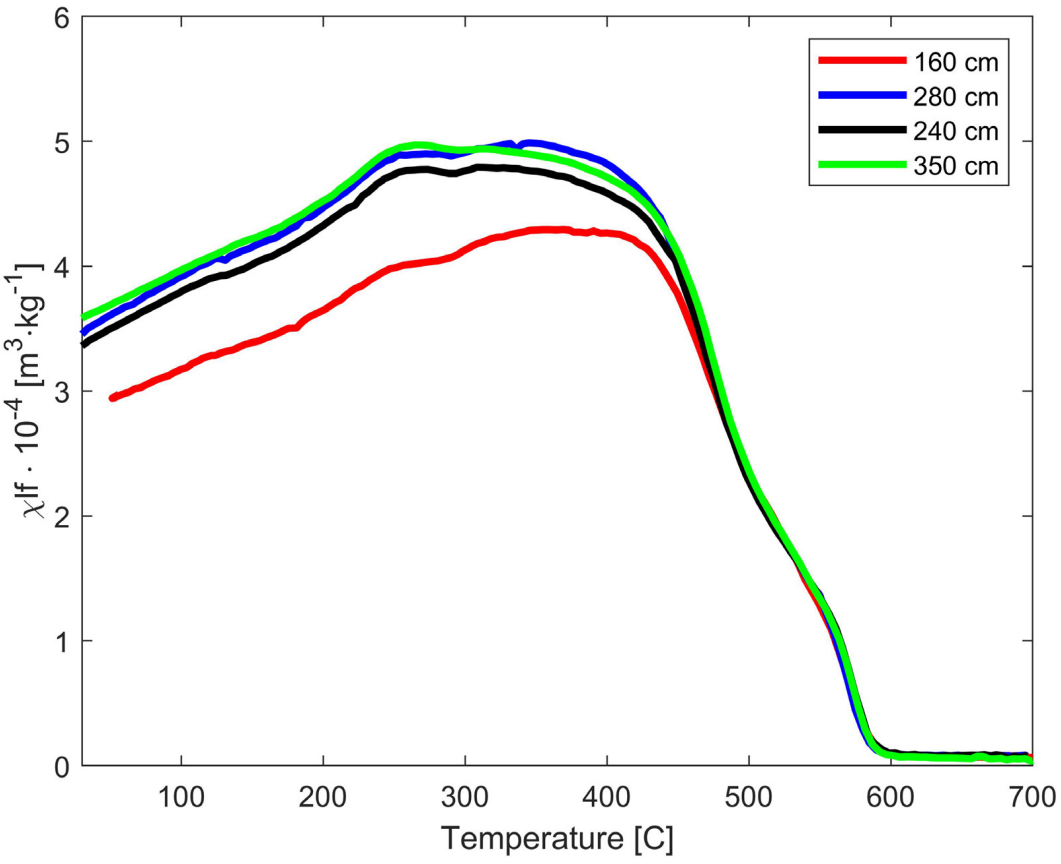

FIGURE 3 | Susceptibility thermomagnetic heating curves.

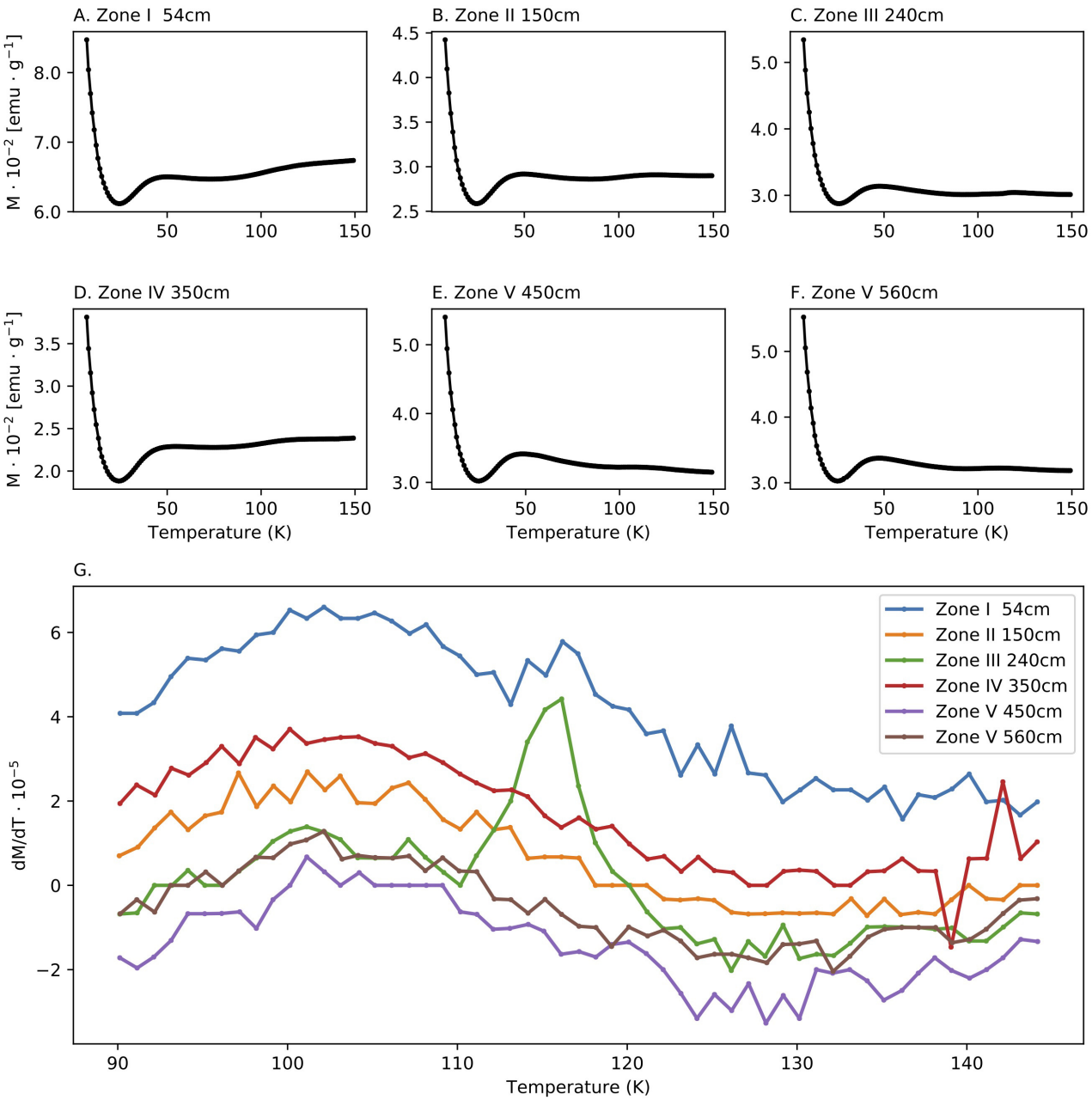

FIGURE 4 | Low temperature measurements. **(A–F)** Zero field cooling (ZFC) curves of samples collected from the five diagenetic zones defines in **(G)** First derivative of the curves shown in **(A–F)** around the Verwey transition temperature.

of stoichiometric magnetite, is observed only at depth of 350 cm. This may suggest low concentration of stoichiometric magnetite in this depth.

Paleomagnetic Directions

Demagnetization of the NRM yielded straight univectorial Zijderveld diagrams with straight lines converging to the origin. ChRM component calculated between 10 mT and 80mT yielded MAD values (Kirschvink, 1980) below 5, typically less than 2, and DANG values (Tauxe and Staudigel, 2004) below 3 (except one specimen). The low MAD indicates low scatter of the data points, and the low DANG values indicate convergence to the origin, which together implies high quality of magnetic recording. We did not observe any correlation between the MAD values and the geochemical zones. To detect the presence of gyro-remanent magnetization (GRM), typical to SD greigite (Snowball, 1997; Roberts et al., 2011) we calculate a GRM(%) parameter (see section "Materials and Methods"). Most of the GRM(%) values (**Figure 2K**) are equal to zero, and except one sample, all values are lower than 2%, indicating no GRM effect in this dataset.

The inclination values (**Figure 2L**) range between 30° and 57°, where the geocentric axial dipole (GAD) inclination in the study area is 52.4°. Thus, the directions fall within the expected secular variation range.

DISCUSSION

Study Site Conditions

Sela-Adler et al. (2015) collected several cores from nearby stations, at water depths of 80–88, across a 10 km N-S trending strip in the vicinity of SG-1 station. In all cores, they identified the SMTZ in the top 4 m of the sediment and a clear signature of *in situ* methane. Following their findings, we investigated in details SG-1, in an attempt to better define the diagenesis zones in the upper sediment and correlate them with the magnetic properties of the sediment. Our interpretations of the new geochemical and magnetic data are based on the assumptions of a steady state condition, that is semi-constant delivery of sediments with similar properties. Generally speaking, there are a number of non-steady state mechanisms that can potentially violate our working assumption. One possible scenario is an abrupt change in the sedimentation rate, which can cause migration of the SMTZ (e.g., Riedinger et al., 2005; Fu et al., 2008). In addition, temporal changes in the organic matter load into the sediment can affect the depths of the different respiration processes (e.g., Larrasoaña et al., 2003; Rowan et al., 2009). Also, changes in the grain size and composition can lead to the accumulation of magnetic minerals in the sediment and change in the magnetic parameters. These mechanisms require time-variations in the flux of the sediment from Nile river, which is the main source of sediments to the studied area. Indeed, the Nile has experienced several environmental changes in the Holocene. The African Humid Period (AHP), which extended from 10–6 kyr was associated with an increased runoff of the Nile river and enhanced supply of organic-rich sediment. The outcome of these changes is the deposition of dark organic-rich sapropel layer (Rossignol-Strick et al., 1982). Yet, the sapropel layer is located at much greater depths below our investigated core. Also, while the Nile river water discharge in the last 6 kyr has changed several times, mainly due to shifts in the Inter-Tropical Convergence Zone (ITCZ), potential changes in the sedimentation rate of the SE Mediterranean have not been observed since by the last sapropel (e.g., Blanchet et al., 2013 for the last 7 kyr).

A number of observations support the steady state assumption. The entire core comprises homogenous lithology of silts and clays (Wurgaft et al., 2019), and the XRD analysis indicates nearly identical composition at all depths (**Supplementary Figure S1**). In addition, the thermomagnetic curves are also nearly identical, supporting the assumption of no significant change in the bulk properties of the sediment source. A physical disturbance of the sediments seems unlikely as the core was collected from a stable part of the continental shelf, where mass transports and turbidity currents do not play a significant role. Indeed, the paleomagnetic data show a stable paleomagnetic recording mechanism and all the paleomagnetic directions fall within the expected range of geomagnetic secular variation. This excludes the possibility of sediment disturbance from currents or slumps.

The sediment in SG-1 site was not dated, and the sequence lacks any chronological marker that enable estimation of the sedimentation rate and the age span of the core. Yet, based on previous analysis of cores from similar depths (Bareket et al., 2016), the estimated deposition rate is around 1 mm/year. To better constrain the age of the core, we show in **Figure 5** the prediction of global geomagnetic models (**Figure 5A**) compared to the paleomagnetic inclination in SG-1 (**Figure 5B**). We used the SHA.DIF.14k geomagnetic model of Pavón-carrasco et al. (2014) that covers the past 14,000 years because it spans through sufficient time interval. The paleomagnetic inclination profile in SG-1 shows a steady decrease in inclination from 200 cm down to the bottom of the core. This trend in SG-1 inclination fits the decrease in inclination from ∼3000 BP to ∼7000 BP. Also, the increase in geomagnetic inclination from ∼9000 BP to the beginning of the Holocene, is not observed in SG-1. This provides us a rough constraint for the maximum age of the magnetic acquisition in SG-1, placing it before ∼9000 BP, likely around ∼6000 BP. The paleomagnetic data support our assumption that the sediments were deposited after the last sapropel in Mediterranean.

From the overall observations we base our interpretation of the data on the assumption that the observed depth-variations in the magnetic parameters, which are sensitive to small changes in the mineralogy and grain-size of the ferromagnetic phase, reflect dissolution and precipitation processes related to diagenesis rather than changes in the sediment supply. While we cannot rule out the possibility of other factors affecting the magnetic properties of the sediment, it seems more likely that that the changes in the magnetic parameters that occur in parallel to changes in the pore water geochemical data are associated with diagenesis. In the following parts, we interpret the combined magnetic-geochemical data in view of early diagenesis zones under steady state conditions.

Microbial Respiration Pathways and Magnetic Diagenetic Zones

Based on the geochemical and magnetic results, the sedimentary column can be divided roughly into five diagenetic zones. These zones are shown in **Figure 6**, with the main geochemical-magnetic depth profiles.

Zone I (0–100 cm depth) is the uppermost part of the sediment. It includes an overlap between the ferruginous and the sulfidic zones, as indicated by the high concentrations of dissolved ferrous iron (**Figure 6A**) and a steady decrease of sulfate concentrations with depth (**Figure 6B**). Based on the results of a previous study on an adjacent core, organoclastic sulfate reduction (OSR) is the main mechanism for sulfate reduction in this zone (Wurgaft et al., 2019). Dissolved sulfide concentrations are below the detection limit there and throughout the sediment core, probably due to precipitation of ferrous iron- sulfide minerals (Wurgaft et al., 2019). Indeed, pyrite framboids were observed in this zone (**Figure 7A**), supporting the presence of sulfide in this depth. The magnetic parameters χlf, χfd, ARM,

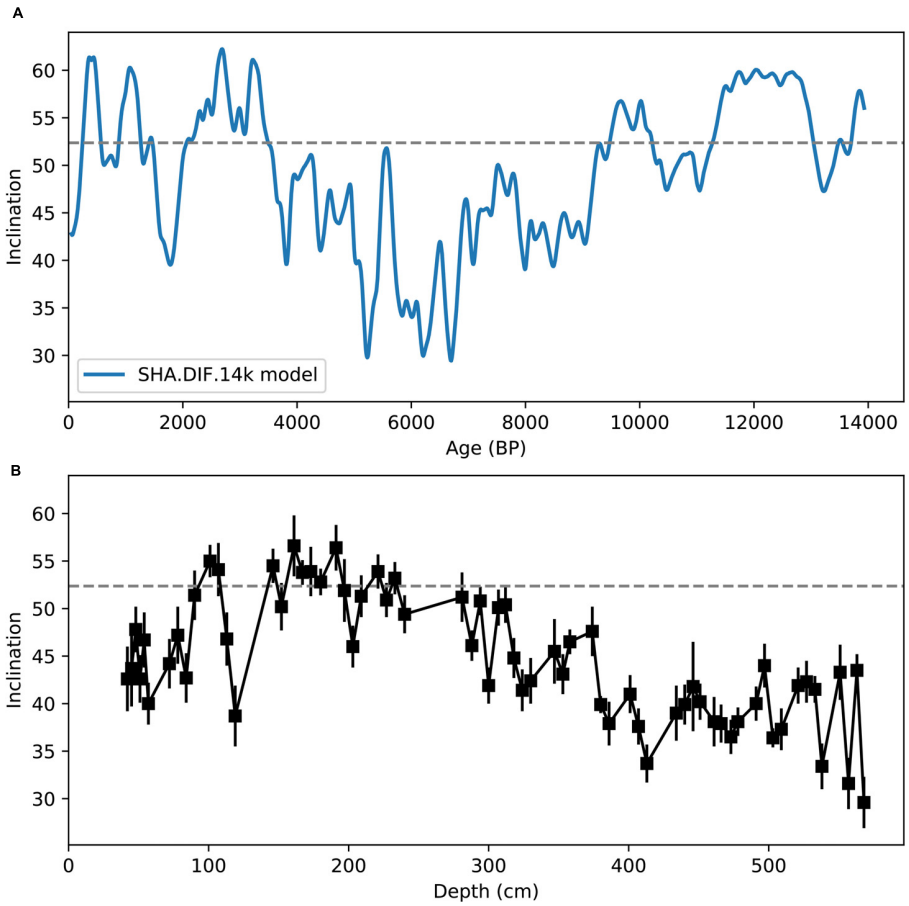

FIGURE 5 | Paleomagnetic inclination. **(A)** Geomagnetic inclination predicted by SHA.DIF.14k model (Pavón-carrasco et al., 2014) at the sampling site. **(B)** Depth profile of paleomagnetic inclinations in SG-1.

and IRM (**Figures 6E–H**) in zone I are high compared to the underlying zones, due to the relatively high concentration of detrital titanomagnetite (**Figure 7B**). A slight increase in the ARM (from 0 to 50 cm) and IRM (from 0 to 90 cm) suggest enhancement of the magnetic parameters, which could potentially be explained by precipitation of ferrimagnetic greigite, or remnants of precursor greigite in pyrite framboids (Ebert et al., 2018), or precipitation biogenic and/or authigenic magnetite (Chang et al., 1987; Karlin et al., 1987; Lovley et al., 1987; Roberts, 2015; Roberts et al., 2018).

Zone II (100–180 cm depth) is the SMTZ, where sulfate concentrations are low and methane concentrations are already measurable. This zone is characterized by intensive sulfate reduction by both anaerobic oxidation of methane (S-AOM) and OSR, which results in sulfide formation (Wurgaft et al., 2019). The sulfide reacts with iron oxides, leading to reductive dissolution of detritus ferric iron minerals and precipitation of the produced dissolved ferrous iron with the excess sulfide, as in Zone I (**Figure 6**). The observed steep decrease in all magnetic parameters in this zone is due to the intense reductive dissolution of iron-bearing magnetic minerals and the precipitation of paramagnetic pyrite (Canfield and Berner, 1987; Rowan and Roberts, 2006; Rowan et al., 2009; Roberts, 2015; Roberts et al., 2018). The frequency dependent susceptibility decreases at a shallower depth than χlf, suggesting that the smaller SD and superparamagnetic (SP) particles dissolve first. The effect of this process on the iron-bearing minerals is displayed in **Figures 7B,C**, showing titanomagnetite with partial dissolution marks and a pyrite framboid.

Zone III (180–310 cm depth) is the upper methanic zone, where sulfate is already depleted, and methane continues to increase with depth. Here we observed another increase in dissolved ferrous iron concentrations, as shown in other methanic sediments (Kawamura et al., 2007; Slomp et al., 2013; Riedinger et al., 2014; Egger et al., 2015). The significant increase in magnetic susceptibility and IRM indicates precipitation of authigenic ferrimagnetic minerals. The sharp increase in frequency-dependent susceptibility indicates a contribution from a large fraction of SP/SD particles. Interestingly, the ARM does not increase as sharply as the susceptibility and the IRM, suggesting that the newly formed particles may be in the non-interacting SD range. As we do not have any direct measurements of this authigenic phase, we can only

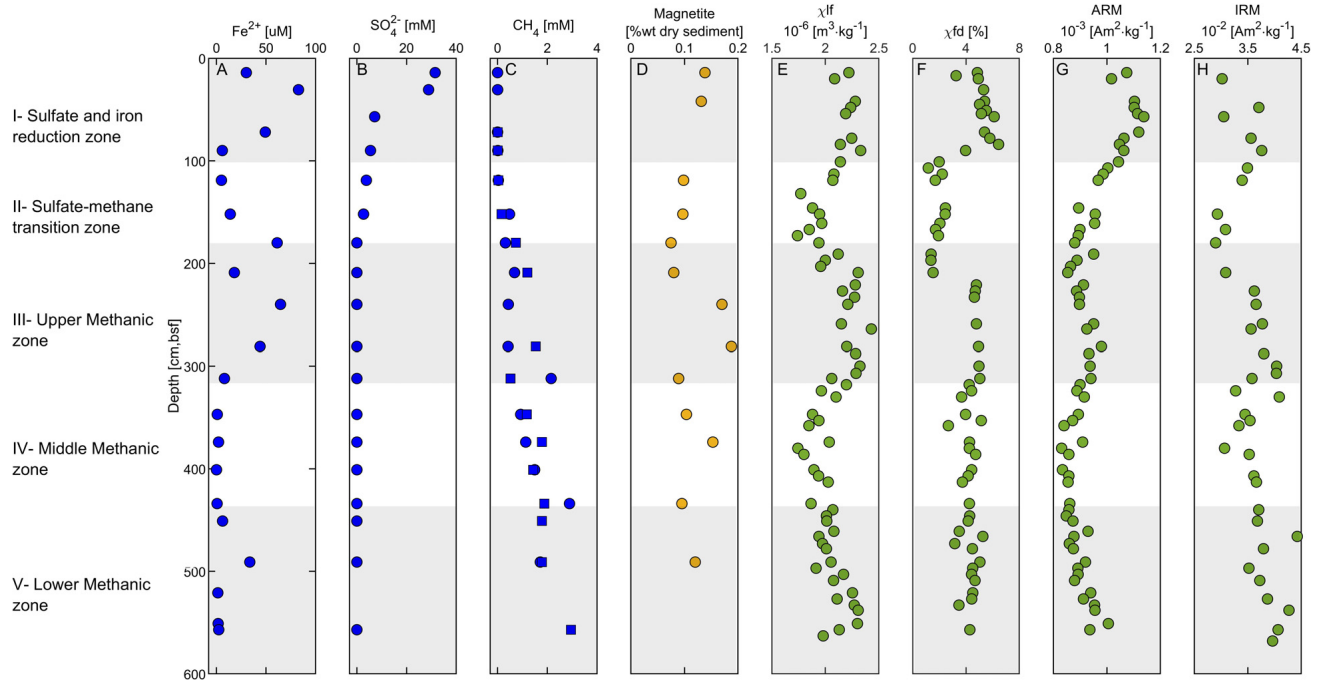

FIGURE 6 | Geochemical – magnetic depth profiles. **(A)** Porewater ferrous iron concentrations. **(B)** Porewater sulfate concentrations. **(C)** Porewater methane concentrations. **(D)** sediment magnetite concentration [following extractions of Poulton and Canfield (2005) protocol]. **(E)** Low-frequency susceptibility, **(F)** Frequency dependent susceptibility. **(G)** Anhysteretic remanent magnetization (ARM). **(H)** Isothermal remanent magnetization (IRM). The data in panels **(A–C)** represent the average of duplicates with error values smaller than the sample symbol, except the methane profile, in which the two duplicates are shown (in squares and circles). The five diagenetic zones are marked with white and gray backgrounds.

hypothesize, in this stage their mineralogy. One possibility is greigite (Larrasoaña et al., 2007; Chang et al., 2008; Rowan et al., 2009; Roberts et al., 2011) or pyrrhotite (Larrasoaña et al., 2007; Roberts, 2015; Horng, 2018; Roberts et al., 2018). Also, authigenic magnetite can explain this type of magnetic pattern, as was shown in the suboxic ferruginous interface (Moskowitz et al., 1989, 1993; Lovley, 1991). The precipitation of authigenic magnetite in this zone is supported by higher magnetite concentrations (**Figure 6D**) and by the largest drop in magnetization next to the Verwey Transition at 120°K (**Figure 4G**). Shang et al. (2020) showed that magnetite can precipitate in anaerobic environments by methanogenic archaeon *Methanosarcina barkeri*, supporting this possibility. The mechanism for its formation remains unknown, although evidence in that work supports the extracellular reduction of ferrihydrite. Electron microscopy from 160 cm depth shows pyrite particles (**Figures 7D,E**) and partly dissolved titanomagnetite (**Figure 7F**), indicating that only part of the detrital titanomagnetite has been dissolved in the SMTZ. Thus, due to the fast sedimentation rate, a significant portion of the detrital ferromagnetic particles survive the SMTZ and can contribute to this diagenetic reaction.

Zone IV (310–575 cm depth) is the middle methanic zone. Here, there are negligible ferrous iron concentrations, methane concentrations still slightly increase with depth, and sulfate is absent. A moderate decrease in χlf, IRM, and ARM is interpreted as further growth and coarsening of the authigenic precipitated magnetic minerals in this zone (Peters and Dekkers, 2003). This can be similar to the results found by Rowan et al. (2009), which suggested that greigite particles in marine sediments grow with depth from superparamagnetic particles through the SD blocking volume.

Zone V (440–575 cm depth) is the lower methanic zone. Ferrous iron concentrations show an increase in one point at 490 cm depth, and methane concentration stops increasing with depth. These observed concertation trends indicate a reduction of ferric iron potentially related to AOM, as previously observed and modeled in the deep methanic depth of marine and freshwater sediments (Sivan et al., 2007, 2011; Riedinger et al., 2014; Egger et al., 2015, 2017; Bar-Or et al., 2017).

The ZFC curves show an increase in the derivative near the Verwey transition temperature mostly in Zone III, indicating the presence of magnetite in a small amount. The occurrence of magnetite could be explained also by greigite oxidation to magnetite following the sediment core extraction. Yet, this does not explain why the Verwey transition is not observed in other zones. Alternatively, it can be a result of direct precipitation of a small fraction of the authigenic magnetite. Interestingly, Verwey transition is not observed in the underlying Zones IV and V, deeper in the methanic zones, suggesting that this magnetite might undergo dissolution at greater depths, fitting the major role of magnetite reduction observed in iron-coupled AOM (Bar-Or et al., 2017). Dissolution can explain the decrease in the magnetic parameters in Zone IV.

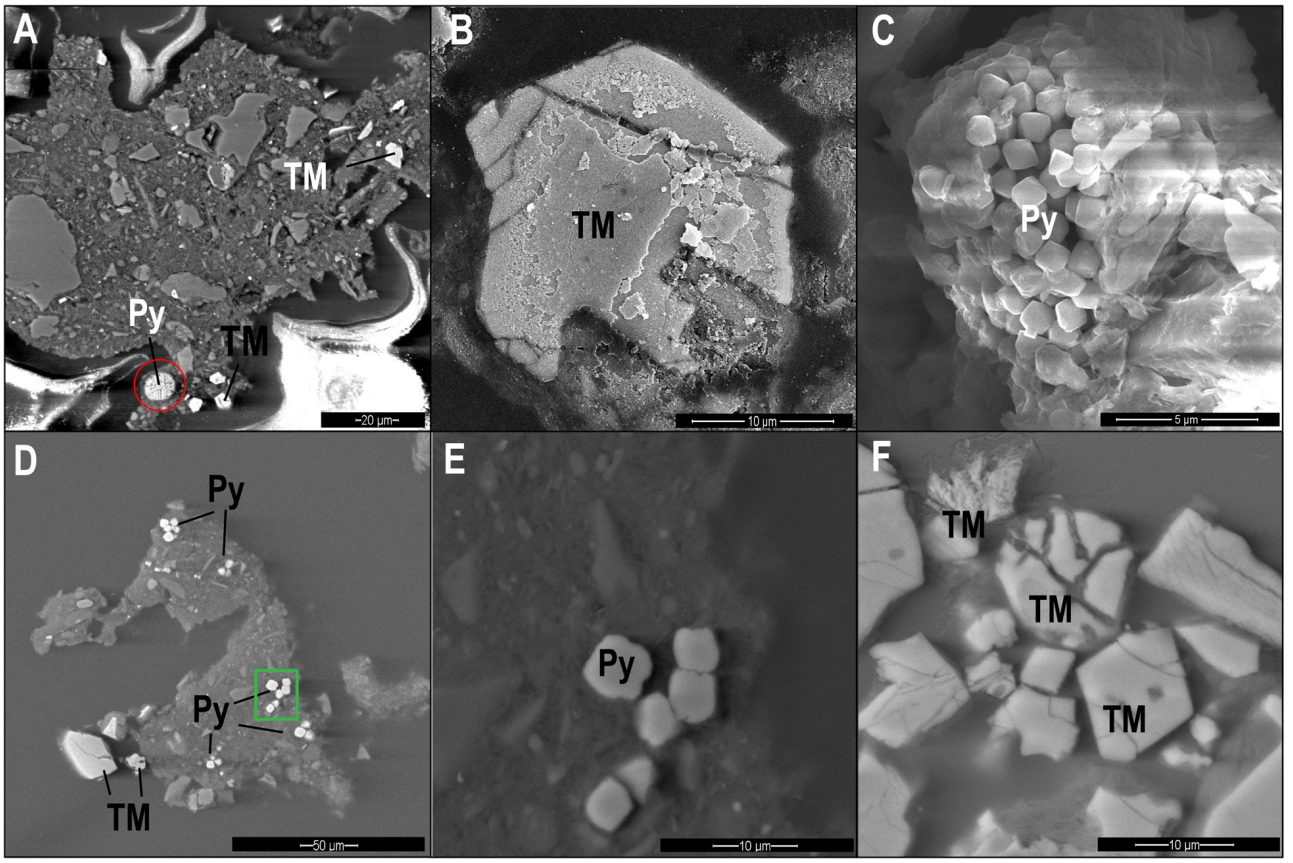

FIGURE 7 | SEM images of pyrite (Py) and titanomagnetite (TM) particles from different diagenetic zones. **(A)** Backscattered electron (BSE) image of pyrite framboid (red circle) and titanomagnetite from Zone I (84 cm depth). **(B)** Secondary electron (SE) image of titanomagnetite with dissolution marks from Zone II (160 cm). **(C)** SE image of a pyrite framboid from Zone II (160 cm). **(D,E)** BSE image of pyrite and titanomagnetite particles from Zone III (280 cm). **(E)** is an enlarged picture of the pyrite region marked with green frame. **(F)** BSE image of partly dissolved titanomagnetite from Zone III (280 cm).

Diagenetic Processes in the Methanic Zone and Their Impact on Magnetic Signals

Microbial iron reduction within the methanic zone has been observed in this area by incubation experiments that included also dead controls (Vigderovich et al., 2019), as well as in other marine provinces (Jørgensen et al., 2004; März et al., 2008; Slomp et al., 2013; Riedinger et al., 2014; Treude et al., 2014; Egger et al., 2015). This means reactivation of iron oxides with low solubility and more crystalline structure, that have "survived" the sulfidic zone at the previously assumed inactive zone, probably in relation to the methane cycling. It is still neither clear why iron oxides are 'reactivated' by the microbes and reduced in these deep methanogenic sediments nor what the link is to methane. However, theoretically, it can be due to the following: (a) Inhibition of methanogenesis by succession competition of iron-reducing bacteria over methanogens at the deeper part due to changes in environmental conditions of processes with close $\Delta G°$ (Jorgensen, 2000; Thamdrup, 2000; Roden et al., 2007). Iron reduction, in this case uses acetate, hydrogen or sulfide, either at low dissolved levels (Vigderovich et al., 2019) or as pyrite or FeS (Bottrell et al., 2000); (b) Direct iron utilization by archaeal methanogens that are abundant in this depth and can reactivate and reduce these low solubility minerals due to their specific advantages in electron transferring (Bond and Lovley, 2002; Van Bodegom et al., 2004; Zhang et al., 2012; Yamada et al., 2014; Sivan et al., 2016); (c) The use of methane, which is present in this zone, as an electron donor for iron reduction. This iron-coupled AOM process was suggested in other marine methanic sediments (Sivan et al., 2007; Riedinger et al., 2014; Treude et al., 2014; Egger et al., 2015, 2016).

The high abundance of iron-oxide minerals that have survived the sulfidic zone for reactivation at the methanic zone can be due to rapid sedimentation rate (Riedinger et al., 2005, 2014; Egger et al., 2017), non-steady state condition in eutrophication conditions (Egger et al., 2015), or intensive methanic zone that shallows the SMTZ zone (Sivan et al., 2007). In our study site, the combination of high sedimentation rates, and high methane fluxes (Vigderovich et al., 2019; Wurgaft et al., 2019) can explain the high concentration of iron-oxide minerals in the deep methanic zone.

The reactivation of iron minerals in the methanic zone means that the traditional view that this zone is magnetically inactive is

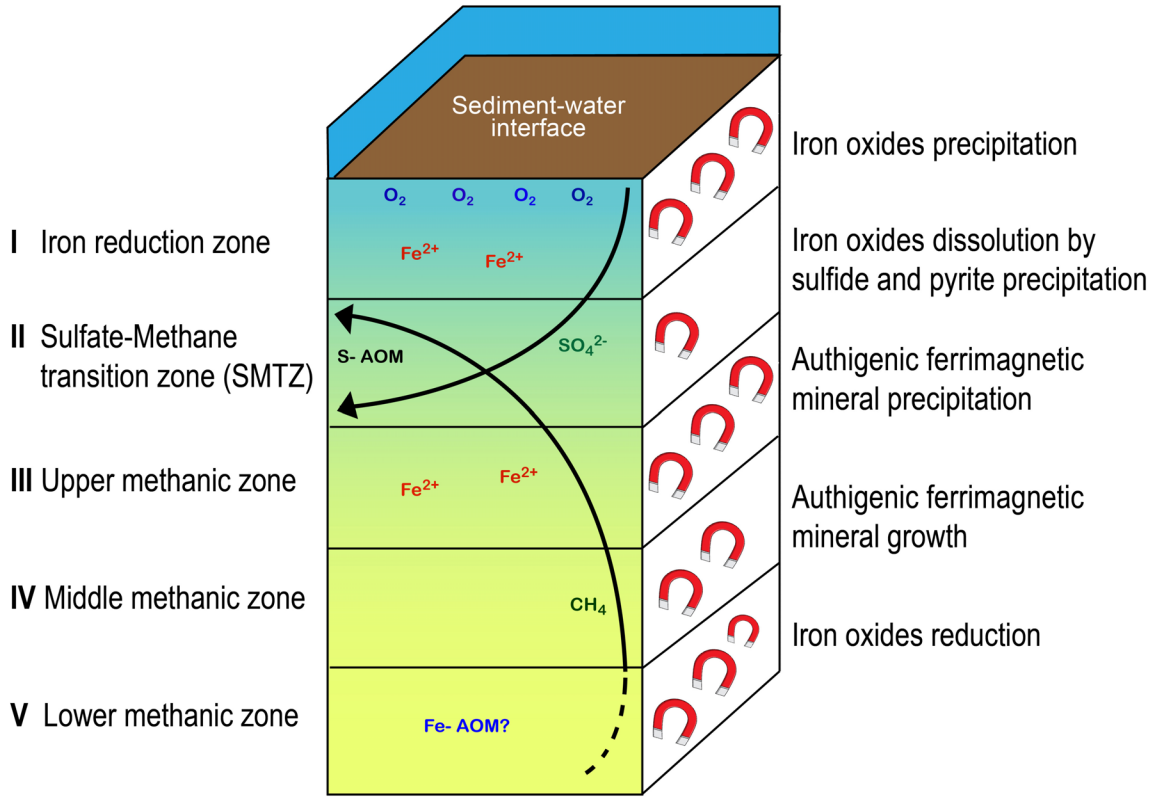

FIGURE 8 | Schematic illustration with a general scheme of the five diagenetic zones, the microbial processes and the resulting magnetic changes in the sedimentary column.

challenged. In this zone only paramagnetic minerals as siderite ($FeCO_3$) and vivianite [$Fe(II)_3(PO_4)\cdot 8H_2O$] were assumed to precipitate under elevated concentrations of dissolved ferrous-iron, if pore waters are saturated with respect to carbonate or phosphate, respectively (Berner, 1980; Slomp et al., 2013; Liu et al., 2018). However, several studies have suggested magnetic modification and mineral precipitation just below the SMTZ, mainly monosulfides, pyrrhotite, greigite and pyrite (Dekkers, 1989; Peters and Dekkers, 2003; Riedinger et al., 2005, 2014; Horng and Chen, 2006; Larrasoaña et al., 2007; Kars and Kodama, 2015; Shi et al., 2017; Horng, 2018; Roberts et al., 2018; Badesab et al., 2019). Here, we show clearly enhancement of the magnetic properties of the upper methanic zone due to precipitation of ferrimagnetic minerals. Sivan et al. (2016) and Shang et al. (2020) studies emphasize the ability of methanogens to reduce iron in anaerobic conditions close to the natural ones in the sediments and to precipitate magnetite as a by-product. These studies may give us a clue about the mechanism for iron reduction in our sediments and the significant precipitation of authigenic ferrimagnetic minerals as magnetite several meters below the surface of the sediments. This precipitation in this zone can cause smoothed remanence acquisition, partial remagnetization or even complete remagnetization (Roberts and Weaver, 2005; Larrasoaña et al., 2007; Rowan et al., 2009; Roberts et al., 2018).

SUMMARY AND CONCLUSION

Our data indicate that early diagenesis can have notable implications on the magnetic parameters of methanic marine sediments. **Figure 8** summarizes the coupling between porewater chemistry and magnetic parameters. Magnetic enhancement is observed first in the classic ferruginous zone. At the SMTZ, the reductive dissolution of magnetic iron minerals, followed by pyrite precipitation, cause a decrease of the magnetic imprint. In the upper methanic zone there is reactivation and reduction dissolution of iron minerals accompanied with intensive precipitation of authigenic ferrimagnetic minerals, enhancing the magnetic parameters of the sediment. In previous studies, pure culture anaerobic experiments close to the natural conditions of methanic sediments showed extracellular precipitation of magnetite, providing a possible explanation for the reactivation of iron minerals in the methanic zone and its potential precipitation there (Shang et al., 2020). This is by a direct switch of methanogens from methanogenesis to iron reduction due to their specific advantages in electron transferring [e.g., through their conductive methanophenazine (Sivan et al., 2016)] and precipitation of magnetite as a by-product. The diagenetic processes described here can potentially contribute

to partial re-magnetization of the sediment and might impact the interpretation of paleomagnetic data. In addition, our data support the understanding that high resolution profiles of rock magnetic parameters, such as IRM, ARM, and susceptibility, can be used to approximate the depth of the SMTZ and the methanic zone in methane-bearing sediments and provide important insights into the degree of magnetic alteration triggered by early diagenesis.

DATA AVAILABILITY STATEMENT

NRM measurements and demagnetization data are available in the MagIC database (earthref.org/MagIC/16844). Geochemical and magnetic depth profile data can be accessed at the PANGAEA repository (https://www.pangaea.de/) (Amiel et al., 2020).

AUTHOR CONTRIBUTIONS

NA wrote the manuscript and analyzed the data. RS and OS planned the research, assisted with data analysis, contributed to discussions, and provided feedback on the manuscript. All authors contributed to the article and approved the submitted version.

FUNDING

The project leading to this application has received funding from the European Union's Horizon 2020 Research and Innovation Program under Grant Agreement Nos. 818450 to OS and 804490 to RS. This project was also supported by the Mediterranean Sea Research Center of Israel to NA and ISF-NSFC grant (2561/16) to OS.

ACKNOWLEDGMENTS

We thank the crew of the RV Bat-Galim and Prof. B. Herut, the head of the Israel Oceanographic and Limnological Research Institute, for their assistance during field sampling and core handling. We also thank Prof. I. Felner from The Hebrew University of Jerusalem, Israel, for his assistance in conducting the low-temperature magnetic measurements, Dr. Valeria Boyko for her help in laboratory work, and Yael Ebert for her assistance with the paleomagnetic measurements.

SUPPLEMENTARY MATERIAL

The Supplementary Material for this article can be found online at: https://www.frontiersin.org/articles/10.3389/feart.2020.00283/full#supplementary-material

REFERENCES

Amiel, N., Shaar, R., and Sivan, O. (2020). Porewater chemistry and magnetic parameters of a sediment core from SG1 station in the South-Eastern Mediterranean Sea. *PANGAEA* doi: 10.1594/PANGAEA.919428

Badesab, F., Gaikwad, V., and Dewangan, P. (2019). Controls on Greigite preservation in a gas hydrate system of the Krishna-Godavari basin, Bay of Bengal. *Geo Mar. Lett.* 124, 4428–4451. doi: 10.1007/s00367-019-00604-z

Bareket, M. M., Bookman, R., Katsman, R., de Stigter, H., and Herut, B. (2016). The role of transport processes of particulate mercury in modifying marine anthropogenic secondary sources, the case of Haifa bay, Israel. *Mar. Pollut. Bull.* 105, 286–291. doi: 10.1016/j.marpolbul.2016.02.014

Bar-Or, I., Elvert, M., Eckert, W., Kushmaro, A., Vigderovich, H., Zhu, Q., et al. (2017). Iron-Coupled anaerobic oxidation of methane performed by a mixed bacterial-archaeal community based on poorly reactive minerals. *Environ. Sci. Technol.* 51, 12293–12301. doi: 10.1021/acs.est.7b03126

Berner, R. (1980). *Early Diagenesis: A Theoretical Approach (No. 1)*. Princeton, NJ: Princeton University Press.

Berner, R. A. (1984). Sedimentary pyrite formation. *Am. J. Sci.* 268, 1–23. doi: 10.2475/ajs.268.1.1

Blanchet, C. L., Tjallingii, R., Frank, M., Lorenzen, J., Reitz, A., Brown, K., et al. (2013). High- and low-latitude forcing of the Nile River regime during the Holocene inferred from laminated sediments of the Nile deep-sea fan. *Earth Planet. Sci. Lett.* 364, 98–110. doi: 10.1016/j.epsl.2013.01.009

Bond, D. R., and Lovley, D. R. (2002). Reduction of Fe(III) oxide by methanogens in the presence and absence of extracellular quinones. *Environ. Microbiol.* 4, 115–124. doi: 10.1046/j.1462-2920.2002.00279.x

Bottrell, S. H., Parkes, R. J., Cragg, B. A., and Raiswell, R. (2000). Isotopic evidence for anoxic pyrite oxidation and stimulation of bacterial sulphate reduction in marine sediments. *J. Geol. Soc.* 157, 711–714. doi: 10.1144/jgs.157.4.711

Canfield, D. E., and Berner, R. A. (1987). Dissolution and pyritization of magnetite in anoxic marine sediments. *Geochim. Cosmochim. Acta* 51, 645–659. doi: 10.1016/0016-7037(87)90076-7

Canfield, D. E., and Thamdrup, B. (2009). Towards a consistent classification scheme for geochemical environments, or, why we wish the term "suboxic" would go away: editorial. *Geobiology* 7, 385–392. doi: 10.1111/j.1472-4669.2009.00214.x

Chang, L., Roberts, A. P., Tang, Y., Rainford, B. D., Muxworthy, A. R., and Chen, Q. (2008). Fundamental magnetic parameters from pure synthetic greigite (Fe3S4). *J. Geophys. Res.* 113:B06104. doi: 10.1029/2007JB005502

Chang, S. B. R., Kirschvink, J. L., and Stolz, J. F. (1987). Biogenic magnetite as a primary remanence carrier in limestone deposits. *Phys. Earth Planet. Inter.* 46, 289–303. doi: 10.1016/0031-9201(87)90191-9

Channell, J. E. T., Freeman, R., Heller, F., and Lowrie, W. (1982). Timing of diagenetic haematite growth in red pelagic limestones from Gubbio (Italy). *Earth Planet. Sci. Lett.* 58, 189–201. doi: 10.1016/0012-821X(82)90193-5

Cline, J. D. (1969). Spectrophotometric determination of hydrogen sulfide in natural waters. *Limnol. Oceanogr.* 14, 454–458. doi: 10.4319/lo.1969.14.3.0454

Cornell, R. M., and Schwertmann, U. (2003). *The Iron Oxides*, 2nd Edn. Weinheim: John Wiley & Sons. doi: 10.1002/9783527613229.ch01

Cruz, A. P. S., Barbosa, C. F., Ayres-Neto, A., Munayco, P., Scorzelli, R. B., Amorim, N. S., et al. (2018). Geochemistry and magnetic sediment distribution at the western boundary upwelling system of southwest Atlantic. *Cont. Shelf Res.* 153, 64–74. doi: 10.1016/j.csr.2017.12.011

Dekkers, M. J. (1989). Magnetic properties of natural pyrrhotite. II. High- and low-temperature behaviour of Jrs and TRM as function of grain size. *Phys. Earth Planet. Inter.* 57, 266–283. doi: 10.1016/0031-9201(89)90116-7

Ebert, Y., Shaar, R., Emmanuel, S., Nowaczyk, N., and Stein, M. (2018). Overwriting of sedimentary magnetism by bacterially mediated mineral alteration. *Geology* 46, 2–5. doi: 10.1130/G39706.1

Egger, M., Hagens, M., Sapart, C. J., Dijkstra, N., van Helmond, N. A. G. M., Mogollón, J. M., et al. (2017). Iron oxide reduction in methane-rich deep Baltic Sea sediments. *Geochim. Cosmochim. Acta* 207, 256–276. doi: 10.1016/j.gca.2017.03.019

Egger, M., Kraal, P., Jilbert, T., Sulu-Gambari, F., Sapart, C. J., Röckmann, T., et al. (2016). Anaerobic oxidation of methane alters sediment records of sulfur, iron

and phosphorus in the Black Sea. *Biogeosciences* 13, 5333–5355. doi: 10.5194/bg-13-5333-2016

Egger, M., Rasigraf, O., Sapart, C. J., Jilbert, T., Jetten, M. S. M., Röckmann, T., et al. (2015). Iron-mediated anaerobic oxidation of methane in brackish coastal sediments. *Environ. Sci. Technol.* 49, 277–283. doi: 10.1021/es503663z

Froelich, P. N., Klinkhammer, G. P., Bender, M. L., Luedtke, N. A., Heath, G. R., Cullen, D., et al. (1979). Early oxidation of organic matter in pelagic sediments of the eastern equatorial Atlantic: suboxic diagenesis. *Geochim. Cosmochim. Acta* 43, 1075–1090. doi: 10.1016/0016-7037(79)90095-4

Fu, Y., von Dobeneck, T., Franke, C., Heslop, D., and Kasten, S. (2008). Rock magnetic identification and geochemical process models of greigite formation in Quaternary marine sediments from the Gulf of Mexico (IODP Hole U1319A). *Earth Planet. Sci. Lett.* 275, 233–245. doi: 10.1016/j.epsl.2008.07.034

Garming, J. F. L., Bleil, U., and Riedinger, N. (2005). Alteration of magnetic mineralogy at the sulfate-methane transition: analysis of sediments from the Argentine continental slope. *Phys. Earth Planet. Inter.* 151, 290–308. doi: 10.1016/j.pepi.2005.04.001

Horng, C. S. (2018). Unusual magnetic properties of sedimentary pyrrhotite in methane seepage sediments: comparison with metamorphic pyrrhotite and sedimentary greigite. *J. Geophys. Res.* 123, 4601–4617. doi: 10.1002/2017JB015262

Horng, C. S., and Chen, K. H. (2006). Complicated magnetic mineral assemblages in marine sediments offshore of southwestern Taiwan: possible influence of methane flux on the early diagenetic process. *Terr. Atmos. Ocean. Sci.* 17, 1009–1026. doi: 10.3319/TAO.2006.17.4.1009(GH)

Jorgensen, B. B. (2000). "Bacteria and marine biogeochemistry," in *Marine Geochemistry*, eds H. D. Schulz, and M. Zabel (Berlin: Springer-Verlag), 169–206. doi: 10.1007/3-540-32144-6_5

Jørgensen, B. B., Böttcher, M. E., Lüschen, H., Neretin, L. N., and Volkov, I. I. (2004). Anaerobic methane oxidation and a deep H2S sink generate isotopically heavy sulfides in Black Sea sediments. *Geochim. Cosmochim. Acta* 68, 2095–2118. doi: 10.1016/j.gca.2003.07.017

Karlin, R., Lyle, M., and Heath, G. R. (1987). Authigenic magnetite formation in suboxic marine sediments. *Nature* 326, 490–493. doi: 10.1038/326490a0

Kars, M., and Kodama, K. (2015). Authigenesis of magnetic minerals in gas hydrate-bearing sediments in the Nankai Trough, offshore Japan. *Geochem. Geophys. Geosyst.* 16, 947–961. doi: 10.1002/2014GC005614.Received

Kasten, S., Freudenthal, T., Gingele, F. X., and Schulz, H. D. (1998). Simultaneous formation of iron-rich layers at different redox boundaries in sediments of the Amazon deep-sea fan. *Geochim. Cosmochim. Acta* 62, 2253–2264. doi: 10.1016/S0016-7037(98)00093-3

Kawamura, N., Ishikawa, N., and Torii, M. (2012). Diagenetic alteration of magnetic minerals in Labrador sea sediments (IODP sites U1305, U1306, and U1307). *Geochem. Geophys. Geosyst.* 13:Q08013. doi: 10.1029/2012GC004213

Kawamura, N., Oda, H., Ikehara, K., Yamazaki, T., Shioi, K., and Taga, S. (2007). Diagenetic effect on magnetic properties of marine core sediments from the southern Okhotsk Sea. *Earth Planets Space* 59, 83–93. doi: 10.1186/bf03352680

Kirschvink, J. L. (1980). The least-squares line and plane and the analysis of palaeomagnetic data. *Geophys. J. Int.* 62, 699–718. doi: 10.1111/j.1365-246x.1980.tb02601.x

Lambeck, K., and Purcell, A. (2005). Sea-level change in the Mediterranean Sea since the LGM: model predictions for tectonically stable areas. *Quat. Sci. Rev.* 24, 1969–1988. doi: 10.1016/j.quascirev.2004.06.025

Larrasoaña, J. C., Roberts, A. P., Musgrave, R. J., Gràcia, E., Piñero, E., Vega, M., et al. (2007). Diagenetic formation of greigite and pyrrhotite in gas hydrate marine sedimentary systems. *Earth Planet. Sci. Lett.* 261, 350–366. doi: 10.1016/j.epsl.2007.06.032

Larrasoaña, J. C., Roberts, A. P., Stoner, J. S., Richter, C., and Wehausen, R. (2003). A new proxy for bottom-water ventilation in the eastern Mediterranean based on diagenetically controlled magnetic properties of sapropel-bearing sediments. *Palaeogeogr. Palaeoclimatol. Palaeoecol.* 190, 221–242. doi: 10.1016/S0031-0182(02)00607-7

Liu, J. (2004). High-resolution analysis of early diagenetic effects on magnetic minerals in post-middle-Holocene continental shelf sediments from the Korea Strait. *J. Geophys. Res.* 109:B03103. doi: 10.1029/2003JB002813

Liu, J., Izon, G., Wang, J., Antler, G., Wang, Z., Zhao, J., et al. (2018). Vivianite formation in methane-rich deep-sea sediments from the South China Sea. *Biogeosciences* 15, 6329–6348. doi: 10.5194/bg-15-6329-2018

Liu, Q., Roberts, A. P., Larrasoaa, J. C., Banerjee, S. K., Guyodo, Y., Tauxe, L., et al. (2012). Environmental magnetism: principles and applications. *Rev. Geophys.* 50:RG4002. doi: 10.1029/2012RG000393

Lovley, D. R. (1991). Dissimilatory Fe (III) and Mn (IV) reduction. *Microbiol. Mol. Biol. Rev.* 55, 259–287. doi: 10.1016/S0065-2911(04)49005-5

Lovley, D. R., Chapelle, F. H., and Phillips, E. J. P. (1990). Fe(III)-reducing bacteria in deeply buried sediments of the Atlantic Coastal Plain. *Geology* 18, 954–957.

Lovley, D. R., Stolz, J. F., Nord, G. L., and Phillips, E. J. P. (1987). Anaerobic production of magnetite by a dissimilatory iron-reducing microorganism. *Nature* 330, 252–254. doi: 10.1038/330252a0

Maloof, A. C., Kopp, R. E., Grotzinger, J. P., Fike, D. A., Bosak, T., Vali, H., et al. (2007). Sedimentary iron cycling and the origin and preservation of magnetization in platform carbonate muds, Andros Island, Bahamas. *Earth Planet. Sci. Lett.* 259, 581–598. doi: 10.1016/j.epsl.2007.05.021

März, C., Hoffmann, J., Bleil, U., de Lange, G. J., and Kasten, S. (2008). Diagenetic changes of magnetic and geochemical signals by anaerobic methane oxidation in sediments of the Zambezi deep-sea fan (SW Indian Ocean). *Mar. Geol.* 255, 118–130. doi: 10.1016/j.margeo.2008.05.013

Moskowitz, B. M., Frankel, R. B., and Bazylinski, D. A. (1993). Rock magnetic criteria for the detection of biogenic magnetite. *Earth Planet. Sci. Lett.* 120, 283–300. doi: 10.1016/0012-821X(93)90245-5

Moskowitz, B. M., Frankel, R. B., Bazylinski, D. A., Jannasch, H. W., and Lovley, D. R. (1989). A comparison of magnetite particles produced anaerobically by magnetotactic and dissimilatory iron-reducing bacteria. *Geophys. Res. Lett.* 16, 665–668. doi: 10.1029/GL016i007p00665

Nir, Y. (1984). *Recent Sediments of the Israel Mediterranean Continental Shelf and Slope*. Gothenburg: Goteborg University.

Nowaczyk, N. R. (2011). Dissolution of titanomagnetite and sulphidization in sediments from Lake Kinneret. Israel. *Geophys. J. Int.* 187, 34–44. doi: 10.1111/j.1365-246X.2011.05120.x

Pavón-carrasco, F. J., Luisa, M., Miquel, J., and De Santis, A. (2014). A geomagnetic field model for the Holocene based on archaeomagnetic and lava flow data. *Earth Planet. Sci. Lett.* 388, 98–109. doi: 10.1016/j.epsl.2013.11.046

Peters, C., and Dekkers, M. J. (2003). Selected room temperature magnetic parameters as a function of mineralogy, concentration and grain size. *Phys. Chem. Earth* 28, 659–667. doi: 10.1016/S1474-7065(03)00120-7

Poulton, S. W., and Canfield, D. E. (2005). Development of a sequential extraction procedure for iron: implications for iron partitioning in continentally derived particulates. *Chem. Geol.* 214, 209–221. doi: 10.1016/j.chemgeo.2004.09.003

Rao, V. P., Kessarkar, P. M., Patil, S. K., and Ahmad, S. M. (2008). Rock magnetic and geochemical record in a sediment core from the eastern Arabian Sea: diagenetic and environmental implications during the late Quaternary. *Palaeogeogr. Palaeoclimatol. Palaeoecol.* 270, 46–52. doi: 10.1016/j.palaeo.2008.08.011

Rickard, D., and Luther, W. G. (2007). Chemistry of iron sulfides. *Chem. Rev.* 107, 514–562. doi: 10.1021/cr0503658

Riedinger, N., Formolo, M. J., Lyons, T. W., Henkel, S., Beck, A., and Kasten, S. (2014). An inorganic geochemical argument for coupled anaerobic oxidation of methane and iron reduction in marine sediments. *Geobiology* 12, 172–181. doi: 10.1111/gbi.12077

Riedinger, N., Pfeifer, K., Kasten, S., Garming, J. F. L., Vogt, C., and Hensen, C. (2005). Diagenetic alteration of magnetic signals by anaerobic oxidation of methane related to a change in sedimentation rate. *Geochim. Cosmochim. Acta* 69, 4117–4126. doi: 10.1016/j.gca.2005.02.004

Roberts, A. P. (1995). Magnetic properties of sedimentary gregite (Fe3S4). *Earth Planet. Sci. Lett.* 134, 227–236. doi: 10.1016/0012-821X(95)00131-U

Roberts, A. P. (2015). Magnetic mineral diagenesis. *Earth Sci. Rev.* 151, 1–47. doi: 10.1016/j.earscirev.2015.09.010

Roberts, A. P., Chang, L., Rowan, C, J., Horng, C., and Florindo, F. (2011). Magnetic properties of sedimentary greigite (Fe3S4): an update. *Rev. Geophys.* 49:RG1002. doi: 10.1029/2010RG000336.1.INTRODUCTION

Roberts, A. P., and Weaver, R. (2005). Multiple mechanisms of remagnetization involving sedimentary greigite (Fe3S4). *Earth Planet. Sci. Lett.* 231, 263–277. doi: 10.1016/j.epsl.2004.11.024

Roberts, A. P., Zhao, X., Harrison, R. J., Heslop, D., Muxworthy, A. R., Rowan, C. J., et al. (2018). Signatures of reductive magnetic mineral diagenesis from

unmixing of first-order reversal curves. *J. Geophys. Res.* 123, 4500–4522. doi: 10.1029/2018JB015706

Roden, E. E., Wetzel, R. G., and Dec, N. (2007). Organic carbon oxidation and suppression of methane production by microbial Fe (III) oxide reduction in vegetated and unvegetated freshwater wetland sediments. *Limnology* 41, 1733–1748. doi: 10.4319/lo.1996.41.8.1733

Rossignol-Strick, M., Nesteroff, W., Olive, P., and Vergnaud-Grazzini, C. (1982). After the deluge: mediterranean stagnation and sapropel formation. *Nature* 295, 105–110. doi: 10.1038/295105a0

Rowan, C. J., and Roberts, A. P. (2006). Magnetite dissolution, diachronous greigite formation, and secondary magnetizations from pyrite oxidation: unravelling complex magnetizations in Neogene marine sediments from New Zealand. *Earth Planet. Sci. Lett.* 241, 119–137. doi: 10.1016/j.epsl.2005.10.017

Rowan, C. J., Roberts, A. P., and Broadbent, T. (2009). Reductive diagenesis, magnetite dissolution, greigite growth and paleomagnetic smoothing in marine sediments: a new view. *Earth Planet. Sci. Lett.* 277, 223–235. doi: 10.1016/j.epsl.2008.10.016

Sagnotti, L., and Winkler, A. (1999). Rock magnetism and palaeomagnetism of greigite-bearing mudstones in the Italian peninsula. *Earth Planet. Sci. Lett.* 165, 67–80. doi: 10.1016/s0012-821x(98)00248-9

Schattner, U., Lazar, M., Harari, D., and Waldmann, N. (2012). Active gas migration systems offshore northern Israel, first evidence from seafloor and subsurface data. *Cont. Shelf Res.* 48, 167–172. doi: 10.1016/j.csr.2012.08.003

Schattner, U., Lazar, M., Tibor, G., Ben-Avraham, Z., and Makovsky, Y. (2010). Filling up the shelf - a sedimentary response to the last post-glacial sea rise. *Mar. Geol.* 278, 165–176. doi: 10.1016/j.margeo.2010.10.006

Sela-Adler, M., Herut, B., Bar-Or, I., Antler, G., Eliani-Russak, E., Levy, E., et al. (2015). Geochemical evidence for biogenic methane production and consumption in the shallow sediments of the SE Mediterranean shelf (Israel). *Cont. Shelf Res.* 101, 117–124. doi: 10.1016/j.csr.2015.04.001

Shang, H., Daye, M., Sivan, O., Borlina, C. S., Tamura, N., Weiss, B. P., et al. (2020). Formation of zero-valent iron in iron-reducing cultures of *Methanosarcina barkeri*. *Environ. Sci. Technol.* 54, 7354–7365. doi: 10.1021/acs.est.0c01595

Shi, L., Squier, T. C., Zachara, J. M., and Fredrickson, J. K. (2007). Respiration of metal (hydr)oxides by Shewanella and Geobacter: a key role for multihaem c-type cytochromes. *Mol. Microbiol.* 65, 12–20. doi: 10.1111/j.1365-2958.2007.05783.x

Shi, M., Wu, H., Roberts, A. P., Zhang, S., Zhao, X., Li, H., et al. (2017). Tectonic, climatic, and diagenetic control of magnetic properties of sediments from Kumano Basin, Nankai margin, southwestern Japan. *Mar. Geol.* 391, 1–12. doi: 10.1016/j.margeo.2017.07.006

Sivan, O., Adler, M., Pearson, A., Gelman, F., Bar-Or, I., John, S., et al. (2011). Geochemical evidence for iron-mediated anaerobic oxidation of methane. *Limnol. Oceanogr.* 56, 1536–1544. doi: 10.4319/lo.2011.56.4.1536

Sivan, O., Schrag, D. P., and Murray, R. W. (2007). Rates of methanogenesis and methanotrophy in deep-sea sediments. *Geobiology* 5, 141–151. doi: 10.1111/j.1472-4669.2007.00098.x

Sivan, O., Shusta, S. S., and Valentine, D. L. (2016). Methanogens rapidly transition from methane production to iron reduction. *Geobiology* 14, 190–203. doi: 10.1111/gbi.12172

Slomp, C. P., Mort, H. P., Jilbert, T., Reed, D. C., Gustafsson, B. G., and Wolthers, M. (2013). Coupled dynamics of iron and phosphorus in sediments of an oligotrophic coastal basin and the impact of anaerobic oxidation of methane. *PLoS One* 8:e62386. doi: 10.1371/journal.pone.0062386

Smirnov, A. V., and Tarduno, J. A. (2000). Low-temperature magnetic properties of pelagic sediments (Ocean Drilling Program Site 805C): tracers of maghemitization and magnetic mineral reduction. *J. Geophys. Res.* 105, 16457–16471. doi: 10.1029/2000jb900140

Snowball, I. F. (1997). Gyroremanent magnetization and the magnetic properties of greigite-bearing clays in southern Sweden. *Geophys. J. Int.* 129, 624–636. doi: 10.1111/j.1365-246x.1997.tb04498.x

Stookey, L. L. (1970). Ferrozine-A new spectrophotometric reagent for iron. *Anal. Chem.* 42, 779–781. doi: 10.1021/ac60289a016

Tauxe, L., Shaar, R., Jonestrask, L., Minnett, R., Koppers, A. A. P., Constable, C. G., et al. (2016). PmagPy: software package for paleomagnetic data analysis and a bridge to the Magnetics Information Consortium (MagIC) Database. *Geochem. Geophys. Geosyst.* 17, 2450–2463. doi: 10.1002/2016GC006307.Received

Tauxe, L., and Staudigel, H. (2004). Strength of the geomagnetic field in the Cretaceous Normal Superchron: new data from submarine basaltic glass of the Troodos Ophiolite. *Geochem. Geophys. Geosyst.* 5:Q02H06. doi: 10.1029/2003GC000635

Thamdrup, B. (2000). Bacterial manganese and iron reduction in aquatic sediments. *Adv. Microb. Ecol.* 16, 41–84. doi: 10.1007/978-1-4615-4187-5_2

Torii, M. (2011). Low-temperature oxidation and subsequent downcore dissolution of magnetite in deep-sea sediments, ODP Leg 161 (Western Mediterranean). *J. Geomagn. Geoelect.* 49, 1233–1245. doi: 10.5636/jgg.49.1233

Treude, T., Krause, S., Maltby, J., Dale, A. W., Coffin, R., and Hamdan, L. J. (2014). Sulfate reduction and methane oxidation activity below the sulfate-methane transition zone in Alaskan Beaufort Sea continental margin sediments: implications for deep sulfur cycling. *Geochim. Cosmochim. Acta* 144, 217–237. doi: 10.1016/j.gca.2014.08.018

Valentine, D. L. (2002). Biogeochemistry and microbial ecology of methane oxidation in anoxic environments: a review. *Antonie Van Leeuwenhoek* 81, 271–282. doi: 10.1023/A:1020587206351

Van Bodegom, P. M., Scholten, J. C. M., and Stams, A. J. M. (2004). Direct inhibition of methanogenesis by ferric iron. *FEMS Microbiol. Ecol.* 49, 261–268. doi: 10.1016/j.femsec.2004.03.017

Verwey, E. J. W. (1939). Electronic conduction of magnetite (Fe_3O_4) and its transition point at low temperatures. *Nature* 144, 327–328. doi: 10.1038/144327b0

Vigderovich, H., Liang, L., Herut, B., Wang, F., Wurgaft, E., Rubin-Blum, M., et al. (2019). Evidence for microbial iron reduction in the methanogenic sediments of the oligotrophic SE Mediterranean continental shelf. *Biogeosciences* 16, 3165–3181. doi: 10.5194/bg-2019-21

Wurgaft, E., Findlay, A. J., Vigderovich, H., Herut, B., and Sivan, O. (2019). Sulfate reduction rates in the sediments of the Mediterranean continental shelf inferred from combined dissolved inorganic carbon and total alkalinity profiles. *Mar. Chem.* 211, 64–74. doi: 10.1016/j.marchem.2019.03.004

Yamada, C., Kato, S., Kimura, S., Ishii, M., and Igarashi, Y. (2014). Reduction of Fe(III) oxides by phylogenetically and physiologically diverse thermophilic methanogens. *FEMS Microbiol. Ecol.* 89, 637–645. doi: 10.1111/1574-6941.12365

Zhang, J., Dong, H., Liu, D., Fischer, T. B., Wang, S., and Huang, L. (2012). Microbial reduction of Fe(III) in illite-smectite minerals by methanogen *Methanosarcina mazei*. *Chem. Geol.* 292–293, 35–44. doi: 10.1016/j.chemgeo.2011.11.003

Conflict of Interest: The authors declare that the research was conducted in the absence of any commercial or financial relationships that could be construed as a potential conflict of interest.